

Faint galaxies in semi-analytic models: how robust are the predictions?

Catarina Lobo^{1,2} and Bruno Guiderdoni¹

¹ Institut d’Astrophysique de Paris, CNRS, 98bis Bd Arago, F-75014 Paris, France

² Osservatorio Astronomico di Brera, via Brera 28, I-20121 Milano, Italy

Received ; accepted

Abstract. In spite of their overall success, semi-analytic models of galaxy formation and evolution predict slopes of luminosity functions which are steeper than the observed ones. This discrepancy has generally been explained by subtle surface brightness effects acting on the observational samples. In this paper, we explicitly implement the computation of surface brightness in a simple semi-analytic model (with standard CDM), and we estimate the effect of observational surface brightness thresholds on the predicted luminosity functions. The crucial free parameter in this computation is the efficiency ϵ of supernova feedback which is responsible for the triggering of galactic winds. With the classical formalism for this process, it is difficult to reproduce simultaneously the Tully–Fisher relation and the flat slope of the observational luminosity function with the same value of ϵ . This suggests that the triggering of galactic winds is a complex phenomenon. The highly uncertain formalism for supernova feedback that is used by semi-analytic models produces large uncertainties in the results. However, once a value of ϵ has been chosen, the various luminosity functions observed in different wavebands (B , r , K) and at different surface brightness thresholds, are consistently reproduced with the surface brightness thresholds quoted by the observers. This seems to show that these observations do see subsamples of the same underlying populations of “sub- L_* ” and dwarf galaxies. The conclusion of this heuristic paper is that a more realistic description of SN feedback is needed, and that surface brightness effects should not be neglected in the modelling of galaxy formation.

Key words: Cosmology – Galaxies: formation – Galaxies: evolution – Luminosity functions

1. Introduction

Significant progress has been recently achieved in the modelling of galaxy formation and evolution through the development of the so-called “*ab initio* semi-analytic models” in which the astrophysics of gas collapse, star formation/evolution and stellar feedback can be explicitly implemented in the hierarchical clustering paradigm (White & Frenk 1991; Lacey & Silk 1991; Lacey *et al.* 1993, Kauffmann *et al.* 1993, 1994; Cole *et al.* 1994; Heyl *et al.* 1995; Kauffmann 1995, 1996; Baugh *et al.* 1996a,b, 1997; Somerville & Primack 1998). These models have been successfully applied to the prediction of the statistical properties of galaxies in the UV, visible and NIR emitted by stars, and, very recently, in the FIR emitted by dust (Guiderdoni *et al.* 1998). In spite of differences in the details, these studies lead to conclusions which are remarkably similar.

However, very little theoretical work has been done so far to implement observational biases in theoretical models of galaxy formation and evolution. Among the various possibilities, surface brightness limits are surely the most important bias, and this is why a detailed study of this specific effect in the framework of semi-analytic models is highly desirable. Namely, one would expect that introducing a surface brightness threshold into the calculation would drastically change the predictions issued for the luminosity functions.

As a matter of fact, this kind of improvement seems to be necessary to solve the issue of the luminosity function. All the observational works concerning field galaxies give luminosity function slopes that are clearly less steep than the predicted value $\alpha \sim -1.7$, although this latter slope already takes into account the astrophysics of star formation/evolution and is significantly shallower than the underlying halo mass distribution with $\alpha \sim -2$. Two different explanations have thus been put forward to account for this mismatch, namely, merging of galaxies or failure of detection due to surface brightness limitations.

(1) Merging of galaxies. Merging could reduce the number of objects in the local universe. This hypothesis has been modelled and tested by Kauffmann *et al.* (1993, 1994), Cole *et al.* (1994), Somerville & Primack (1998), and other papers in these series. The results seem to indicate that the merging rate is relatively small and that mass and luminosity functions issued from these models are not significantly different from those computed with less elaborate formalisms.

(2) Failure of detection due to surface brightness limitations. Observational selection effects would provide a simple explanation that could interplay with the strong intrinsic dimming of some galaxies along their lives (see *e.g.* McGaugh 1994; Schade & Ferguson 1994; Phillipps & Driver 1995; Driver & Phillipps 1996; Bothun, Impey & McGaugh 1997). For instance, a strong episode of star formation followed by mass loss due to supernova-driven winds and the aging of the remaining stellar population would cause this dimming and could even eventually lead to the extreme case of gravitational disruption, especially for dwarf or extended galaxies, where the potential well is shallower (Broadhurst *et al.* 1988, Lacey & Silk 1991, Cowie *et al.* 1991, Babul & Rees 1992). This kind of scenarios would also provide a plausible explanation for the differences between field and cluster galaxy luminosity functions, these latter ones showing typically steeper faint-end slopes. As suggested by *e.g.* Babul & Rees (1992), mass loss suffered by galaxies within clusters is actually minimized thanks to the confinement provided by the surrounding intra-cluster gas. In fact, while steep slopes $\alpha \sim -1.8$ of luminosity functions have lately begun to be unveiled by new observations of clusters (*e.g.* Driver *et al.* 1994; De Propris *et al.* 1995; Lobo *et al.* 1997; Wilson *et al.* 1997; Trentham 1997a,b, 1998a,b), it is not clear yet whether field galaxy luminosity functions in the local universe follow the same trend. This is because faint and diffuse objects are marginally detected in the standard spectroscopic surveys of field galaxies and, for those that are flagged, the signal-to-noise ratio is often quite weak.

The nature of these galaxies that fail to be detected by local field surveys is extensively discussed in recent literature (see *e.g.* McGaugh 1995; Bothun, Impey & McGaugh 1997) and they span a large range in mass : from low-mass faint dwarfs till the most massive, low surface brightness, blue disks (*e.g.* Malin 1 ; Bothun *et al.* 1987). These objects do exist in large numbers, even though they contribute somewhat modestly (by 10 to 30%) to the total integrated luminosity (McGaugh & Bothun 1994, Impey *et al.* 1996, McGaugh 1996). Thus, systematic errors undoubtedly affect the field luminosity functions that have been published up to now, since none of them has had a completeness correction to account for this bias (Impey *et al.* 1996). Once the surface brightness selection effects are taken into account, the faint slope of the observed local field luminosity function is bound to suffer a considerable change (McGaugh *et al.* 1995). Computations by Driver

& Phillipps (1996) predict an upturn in the luminosity function at $\mathcal{M}_B > -18$ ¹ that has actually been detected by the works of Schade & Ferguson (1994), Marzke *et al.* (1994a,b) and Zucca *et al.* (1997). The works of Sprayberry *et al.* (1997) and Loveday (1997) also seem to indicate that the local field luminosity function definitely contains more faint members than had been detected up to recently by *e.g.* Loveday *et al.* (1992), Ellis *et al.* (1996), and Lin *et al.* (1996).

It would thus seem that a fading scenario is the most promising approach to tackle the disagreement between theories and observations. In the following, we revisit this problem and analyze the effects of observational biases by comparing the results of galaxy modelling and observations. More specifically, by adopting a scenario of surface brightness dimming, we aim at quantifying the influence of pre-determined surface brightness thresholds on the slope of the multi-wavelength luminosity function of field galaxies.

This issue leads us immediately to consider the delicate modelling of mass loss due to supernova-driven winds. All semi-analytic models use the same ideas to implement this process, originating in the pioneer paper by Dekel & Silk (1986). Type II/Ib supernovae eject kinetic and thermal energy in the interstellar medium. Only a fraction ϵ effectively heats up the gas. When the thermal velocity of the gas reaches the escape velocity v_{esc} , the interstellar medium is lost through galactic winds, and star formation is quenched. The first problem with this standard modelling is that the process depends on the depth of the potential well. In principle, the latter is computable *e.g.* in CDM cosmologies. But the question is whether the theoretical density profiles actually reproduce the true density profiles of haloes. Second, radiative losses are important and, consequently, the efficiency ϵ should be weak (Thornton *et al.* 1998). Finally, this model does not describe what actually occurs in disk galaxies: when the expanding shell reaches the edge of the disk along the z -axis perpendicular to the plane, it simply blows its hot gas out, with little effect on the cold gas of the disk. As a matter of fact, energetic outflows observed in irregular galaxies seem to blow out only a small fraction of the interstellar medium (Martin 1996).

When a surface-brightness criterion is taken into account, the strong uncertainty in the modelling of supernova feedback appears more clearly. Then we can test the robustness of the results at the faint end of the luminosity function. Hereafter, we take the standard model which is used by all authors of semi-analytic models (see the above-mentioned references), and we show how the efficiency parameter ϵ (taken as a “fudge factor”) influences the results. Of course, a still larger uncertainty in the

¹ All values presented throughout this paper have been converted to $H_0 = 50 \text{ km s}^{-1} \text{ Mpc}^{-1}$.

model (which appears plausible) would affect the results to a larger extent.

To achieve this heuristic work, we do not need a complicated cosmological model. We hereafter use a simple version of a semi-analytic model of galaxy formation and evolution, with standard CDM (the most classical case). The layout of this paper is the following : in section 2 we rapidly describe the model, emphasizing the new components we introduce with this work. These determine the behavior of the output quantities relatively to the star formation histories, wind efficiency and surface brightness thresholds, as discussed in section 3. Synthetic luminosity functions are compared with observational data for redshift $z = 0$ in section 4. Finally, in section 5, we discuss the results and present our conclusions. In particular, the shape of the luminosity function provides us with a powerful tool for emphasizing the strong influence of supernova feedback on the detection of faint galaxies when surface brightness criteria are taken into account.

2. The model

We use a simple version of a semi-analytic model of formation and evolution of galaxies, to which we add some original ingredients which are relevant for our study. In this section we will sketch an overview of the underlying model, leaving the detailed descriptions for the new modules introduced by this work. We adopt the standard Cold Dark Matter (SCDM) scenario – namely, a density parameter $\Omega_0 = 1$, a baryon fraction $\Omega_{baryon} = 0.05$, a cosmological constant $\Lambda = 0$, a Hubble constant $H_0 = 50 \text{ km s}^{-1} \text{ Mpc}^{-1}$, and a normalization for the power spectrum of linear fluctuations that is given by the inverse of the linear bias parameter $b = 1.6$ – and we focus on the astrophysics of galaxy evolution. The influence of the cosmological parameters on the predictions of semi-analytic models is studied by *e.g.* Heyl *et al.* (1995) and Somerville & Primack (1998), and turns out to be smaller than the uncertainties due to the free parameters of the dissipative astrophysics (mainly star formation and stellar feedback).

2.1. Dark matter halos

Simplifying assumptions need to be made in a semi-analytic formalism. In particular, the initial linear density perturbation is assumed to be spherical and homogeneous. This is the so-called “top-hat” model, which can be entirely defined by two parameters : the size R and density contrast $(\delta\rho/\rho)_{z=0} \equiv \delta_0$, which are the linearly-extrapolated values at $z = 0$, or, equivalently, by the mass M and collapse redshift z_{coll} . If ρ_0 is the current mass density of the universe, we have $M = (4\pi/3)R^3\rho_0$ and $\delta_0 = \delta_{0c}(1 + z_{coll})$ with $\delta_{0c} = 1.68$ (for $\Omega_0 = 1$). The perturbation thus generated grows, reaches turnaround radius, decouples from the expansion of the Universe and

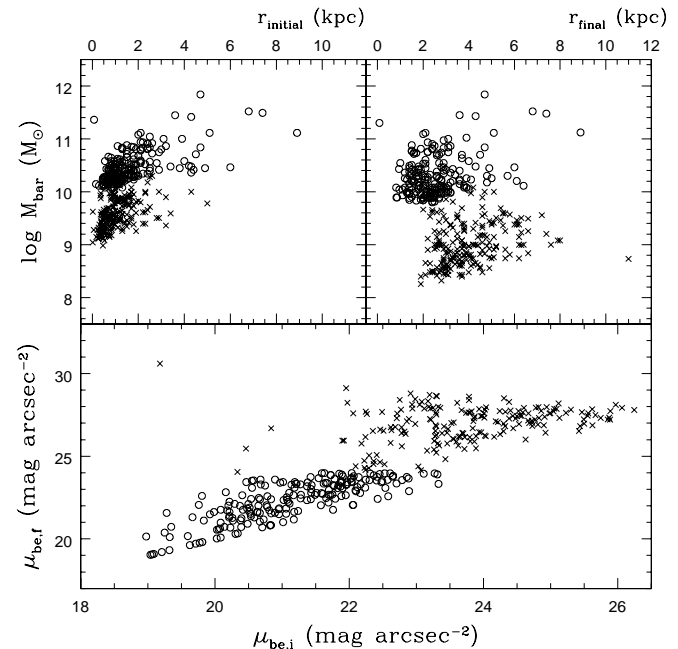


Fig. 1. Figure showing the effect of winds upon the radius of each galaxy, its baryonic mass M_{bar} and its surface brightness (measured at the effective radius in the b_J band). Open circles represent objects that are brighter at $z = 0$ than the critical magnitude and surface brightness thresholds (set by observations) and inversely for crosses. The fudge parameter for supernova feedback is $\epsilon = 0.8$, and the surface-brightness threshold is $\mu_{b,J} = 24 \text{ mag arcsec}^{-2}$. In the upper panels, *initial* denotes the epoch just prior to star formation ignition; at that time, the baryonic mass is taken as all the initial gas mass available to form stars. Subscript *final* corresponds to the present time ($z = 0$), when the baryonic matter is the stellar content plus the remaining gas. In the lower panel, *f* is for *final*, while $\mu_{\text{be},i}$ denotes the surface brightness that the galaxy would have without radial expansion.

collapses to form a spherical, virialized halo truncated at “virial radius” $r_V = 3R/10\delta_0$.

The properties of the virialized halo are entirely computable as functions of M and z_{coll} . Hereafter we adopt the universal density profile proposed by Navarro, Frenk & White (1997, hereafter NFW) instead of the r^{-2} “isothermal” profile, since the former is now used by the most recent versions of the semi-analytic models. Our purpose is to show the uncertainties in the standard situation, rather than to address the issue of the “true” density profile. Anyhow, we checked that the use of “isothermal” profiles would not change our conclusions qualitatively. In the NFW model, the density profile of the relaxed halo at $r \leq r_V$ is :

$$\frac{\rho_H(r)}{\rho_{\text{crit}}} = \frac{\delta_{\text{char}}}{(r/r_s)(1 + r/r_s)^2} \quad (1)$$

where r_s is a scale radius, and $\rho_{crit} = 3H^2/8\pi G$ is the critical density for closure. The characteristic density δ_{char} is computed by:

$$\delta_{char}(M, z_{coll}) \sim 3 \times 10^3 \Omega(z_{coll}) \left(\frac{1 + z_{coll,sub}}{1 + z_{coll}} \right)^3 \quad (2)$$

where $z_{coll,sub}$ is computed according to the procedure described in Navarro, Frenk & White (1997) with $f=0.01$. The ‘‘concentration’’ of a halo, $c = r_V/r_s$, is linked to the characteristic density δ_{char} by means of the definition of the virial radius so that :

$$\delta_{char} = \frac{200}{3} \frac{c^3}{[\ln(1+c) - c/(1+c)]} \quad (3)$$

This implies that the ‘‘circular velocity’’ at radius r is given by :

$$\left(\frac{v_c(r)}{v_{200}} \right)^2 = \frac{1}{x} \frac{\ln(1+cx) - (cx)/(1+cx)}{\ln(1+c) - c/(1+c)} \quad (4)$$

where $v_{200} \equiv (GM/r_V)^{1/2}$ is the velocity at the virial radius, and $x = r/r_V$ is the radius in units of virial radius. The number density of halos that collapse at a given redshift/time and with a given mass is easily determined from a simple Press–Schechter (PS) prescription (Press & Schechter 1974).

$$n(M, z)dM = \sqrt{2/\pi}(\rho_0/M^2)(\delta_{0c}(1+z)/\sigma_0(M)) \times |d \ln \sigma_0(M)/d \ln M| \times \exp -(\delta_{0c}(1+z)^2/2\sigma_0(M)^2) dM \quad (5)$$

If the power spectrum can be approximated by a power law $P(k) \propto k^n$, the low–mass end is $n(M)dM \propto M^{(n-9)/6}dM$. The CDM spectral index varies between -3 and 1 , yielding a slope $\gamma = -2$ to -1.67 , close to -2 on galaxy scales.

We intend hereafter to use a simple prescription and focus on the astrophysics of galaxy formation and evolution. This will make the comparison with previous papers easier. In order to implement the simpler PS formalism, crude assumptions must be done. As a matter of fact, we need the formation rate of haloes versus time or redshift, while the time derivative of the PS number density only gives the net creation rate of haloes with mass M :

$$dn(M, z)/dt = dn_{for}(M, z)/dt - dn_{des}(M, z)/dt \quad (6)$$

The first term of the right–hand part of the equation describes the formation of haloes with mass M from haloes with masses $< M$, while the second term describes the destruction rate to haloes with masses $> M$. For a given mass, the formation rate first dominates ($dn(M, z)/dt > 0$), then the destruction rate dominates ($dn(M, z)/dt < 0$). As *e.g.* in Haehnelt & Rees (1993), we

chose to take $dn_{for}(M, z)/dt = dn(M, z)/dt$ in the first case (destruction is neglected), and 0 in the second case (formation is neglected), to estimate the space density of newly formed haloes. This crude assumption leads to neglecting the effect of galaxy merging which anyway seems to be weak.

2.2. Gas cooling and dissipative collapse

Hierarchical theories of structure formation require a feedback mechanism in order to prevent most of the material from collapsing into sub-galactic objects at high redshifts (*e.g.* Efstathiou 1992). So, we introduce a cut–off at low circular velocities and high redshifts preventing gas cooling if $v_{200} < 100 \text{ km s}^{-1}$ and $2 < z_{coll} < 10$. As shown by Kauffmann *et al.* (1993), this does not alleviate the problem of the dwarfs.

The previously shock–heated baryon component starts cooling down in the potential wells of dark matter haloes and collapses into disks. The cooling time at a given halo radius is computed according to Fall & Rees (1985) and leads to the definition of a cooling radius (r_{cool}) as a function of redshift. At this redshift, only gas inside the cooling radius (or the virial radius, in case the latter is smaller) cools and is available for star formation. Normally, the cooling process depends on gas metallicity but here we do not take this dependence into account, and we shall only consider the solar metallicity case. If we assume angular momentum conservation, then the collapse of the baryonic matter stops when rotational equilibrium is reached. An exponential disk forms. To determine the final radius of the disk relatively to the initial radius of the halo, we apply the formalism proposed by Fall & Efstathiou (1980), and Mo, Mao & White (1998), under the standard assumption that the disk and halo share the same specific angular momentum, even though numerical simulations (Navarro & White 1994, Navarro & Steinmetz 1997) seem to hint that this may be too crude. The typical length scale r_0 for the exponential disk is, again following Mo, Mao & White (1998) :

$$r_0 = \lambda \min(r_V, r_{cool}) f(c, m_d, \lambda) \quad (7)$$

where f is a function of the dimensionless spin parameter λ , the halo concentration factor c , and the fraction m_d of the halo mass that settles into the disk. A sufficiently accurate approximation (Mo, Mao & White 1998) to f is :

$$f \approx \left(\frac{\lambda}{0.1} \right)^{-0.06+2.71m_d+0.0047/\lambda} (1 - 3m_d + 5.2m_d^2) \times (1 - 0.019c + 0.00025c^2 + 0.52/c), \quad (8)$$

We note that only disks and dwarfs can form in this formalism. As we previously mentioned in section 1, the formation of elliptical galaxies (and of bulges of spiral galaxies) has to be explained by the merging of disks. Kauffmann *et al.* (1994) and Cole *et al.* (1994) showed

that this merging process can easily explain the current fraction of giant ellipticals among bright galaxies (about 10 %).

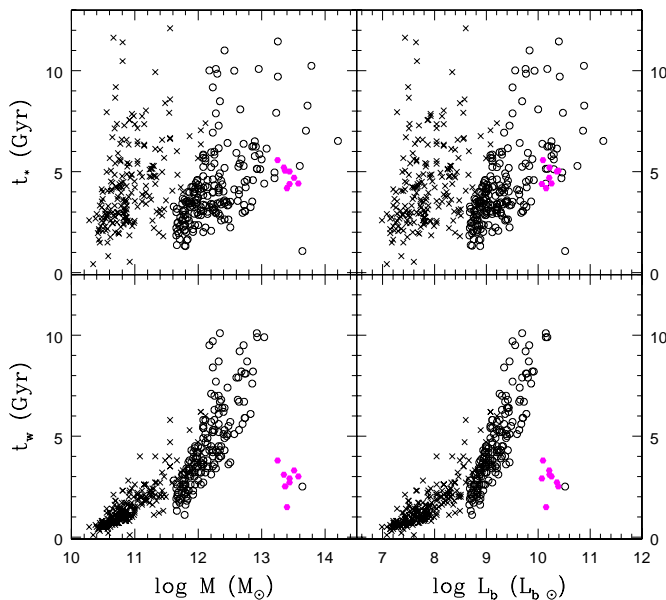


Fig. 2. The characteristic time scale for star formation t_* and the age at which each galaxy has its first wind t_w as a function both of the halo mass (left-hand panels) and blue luminosity (right-hand panels). The free parameters and symbols are the same as in figure 1 except for the newly added filled circles, which account for a particular class of high luminosity, low surface brightness, galaxies (see text for details). Only galaxies that have winds have been plotted in the bottom panels

2.3. Star formation rate and initial mass function

Stars begin to form with the gas available inside the cooling (or the virial) radius according to a given star formation rate $\psi(t)$. Here we shall consider a simple case of direct proportionality to the gas surface density Σ_{gas} , which seems to be supported by the latest observational evidence (Kennicutt 1998). We also introduce a critical threshold Σ_c , according to Toomre (1964) and Kennicutt (1989). We here adopt the numerical value determined by Kennicutt (1989) for an ensemble of disks :

$$\Sigma_c (M_\odot pc^{-2}) \simeq 0.40 v_{200} (km s^{-1}) / r_{disk} (kpc) \quad (9)$$

knowing that the half-mass radius of an exponential disk is :

$$r_{disk} = 1.68 r_0 \quad (10)$$

This will prevent star formation from occurring whenever the gas surface density is below this limit. Otherwise we have :

$$\psi(t) = \frac{\Sigma_{gas}(t)}{t_*} \quad (11)$$

with t_* derived from the core dynamical times as :

$$t_* = \beta t_{dyn,disk} \quad (12)$$

Here β is a free parameter defining the efficiency of star formation per dynamical time,² and :

$$t_{dyn,disk} = \frac{r_{disk}}{v_{200}} \quad (13)$$

After their formation, stars are placed on the zero-age main sequence of the HR diagram according to an initial mass function. In this work we have chosen to describe the initial mass function by the standard form $\phi(m) \propto m^{-x}$ with slope $x = 1.7$ for stars more massive than $2 M_\odot$ (Scalo 1986), the Salpeter slope $x = 1.35$ for masses between 1 and $2 M_\odot$, and $x = 0.25$ below $1 M_\odot$. A model of spectro-photometric evolution (Guiderdoni & Rocca-Volmerange 1987, 1988 and Rocca-Volmerange & Guiderdoni 1988) issued for a burst of 0.1 Gyr duration with upgraded tracks from Schaller *et al.* (1992) and Charbonnel *et al.* (1996) is used to compute the mass/luminosity ratios and the colors of each generation of stars according to their age. Then the burst evolution is convolved with the star formation rate history of each galaxy.

2.4. Feedback processes

The mechanism of star formation itself is regulated by feedback due to the explosion of massive stars. The standard modelling of feedback due to supernovae in semi-analytic models of galaxy formation is the following: supernova-driven winds expel gas from the galaxy and, as a consequence, less star formation occurs (Larson 1974, Dekel & Silk 1986, Bressan *et al.* 1994). To determine the time t_w when the galaxy loses its gas mass, we keep track of the balance between the total supernova input energy, responsible for the heating of the inter-stellar medium, and the energy required to eject the gas from the radius r of a galaxy at time t_w :

$$\frac{1}{2} M_{gas}(t_w) v_{esc}(r)^2 = \epsilon \int_0^{t_w} E_{SN} \frac{dN_{SNII}(t)}{dt} dt \quad (14)$$

considering that :

$$\int_0^{t_w} \frac{dN_{SNII}(t)}{dt} dt = \eta_{SN} M_*(t_w) \quad (15)$$

² Do notice, when comparing definitions, that our β parameter here is the Guiderdoni *et al.* (1998) one divided by 2π .

The gas escape velocity $v_{esc}(r)$ at radius r is computable for the NFW profile :

$$\left(\frac{v_{esc}(r)}{v_{200}}\right)^2 = \frac{2 \ln(1+cx) - (cx)/(1+c)}{x \ln(1+c) - c/(1+c)} \quad (16)$$

It is estimated at the half-mass radius r_{disk} . Here E_{SN} is the input energy per supernova, and η_{SN} is the number of supernovae per unit mass of formed stars that depends on the initial mass function. We adopt the standard values $E_{SN} = 10^{51}$ erg, and $\eta_{SN} = 4 \times 10^{-3} M_{\odot}^{-1}$ (computed for our assumed IMF). The Type II/Ib supernovae formation rate $dN_{SNII}(t)/dt$ is computed from the star formation rate history. All models deliberately neglect the contribution from Type Ia. A fine-tuning “efficiency factor” $0 \leq \epsilon \leq 1$ is generically introduced to account for the fraction of the energy that is radiated away and lost by the system. Numerical simulations (Thornton *et al.* 1998) seem to privilege $\epsilon \sim 0.1$. In fact, the efficiency parameter could be still smaller in disk galaxies because of the geometry that allows supernova bubbles to blow out. In section 3.2 we will analyze and discuss the behavior of our model with this parameter which is always used as a “fudge factor”.

2.5. Expansion of the stellar disk

When a galaxy loses mass, this process can occur either impulsively - when the material is ejected within a time scale that is short compared to the dynamical time of the system -, or adiabatically - when mass loss proceeds gradually. In our models we have chosen to consider the first approach only, which seems the most realistic. This implies that the velocities of the stars are not affected during the whole process and their velocity dispersion immediately after the (impulsive) mass loss is the same as it was before. A straightforward consequence of mass loss is a shallowing of the system’s potential. Stars will start describing larger orbits. This translates into a radial expansion of the stellar material of the disk, that we treat here according to Hills (1980). Note that this extension of the galactic radius is crucial for surface brightness considerations as it leads to surface brightness dimming. The final radius of the stellar material, which will allow us to determine the surface brightness of each galaxy after mass loss, is related to the initial radius by equation :

$$\frac{r_f}{r_i} = \frac{M_f}{2 \left[\frac{M_i}{2} - (M_i - M_f) \right]} \quad (17)$$

where the i subscript stands for initial values and f for final ones, after mass loss has occurred. All variables of this equation have been defined at half-mass radius, and r_i refers to the initial stellar radius obtained from the halo radius by means of the (dimensionless) spin parameter (see equations 10 and 7).

2.6. Surface-brightness threshold

Finally, we shall introduce both a flux limit and a surface-brightness threshold that simulate observational limits and we analyze the behavior and sensitivity of our model predictions to these effects (section 4). In fact, it is often the case that the isophote taken to compute the surface brightness limit of a given survey may (1) differ slightly from galaxy to galaxy (if it depends on the magnitude or the size of the object); (2) depend on selection criteria (if the filter used for target selection is not the same as the one used to compute the luminosity function); (3) vary for different images of one same field taken in different nights and/or under different observational conditions. These effects can lead to differences of up to 1 magnitude (E. Bertin, private communication). As a reasonably fair approximation, the surface-brightness limit imposed in our models is computed at the effective radius r_e . Of course, surface-brightness effects are likely to be more subtle than a simple surface-brightness “cut-off”. But little more can be done from the description of the observations provided in the literature.

2.7. Monte-Carlo realizations

We present in this section some of the results of the model described above for output redshift $z = 0$, while emphasizing the surface brightness effects that we want to explore (presented in section 1). One could represent these results by a mean value plus 1σ “error bars” but, because of the non gaussianity of the distributions, this would be somewhat misleading. So, we preferred to draw Monte-Carlo realizations of the model. Thus, in the set of figures that follow, we represent a given number of objects (realizations), separating them accordingly to a magnitude and surface brightness criterion established by observational limits.

Both classes of objects are represented in equal numbers (e.g. 200 of each). Unless stated otherwise, we have adopted limits $\mu_{b,J} = 24$ mag arcsec⁻² and absolute magnitude $\mathcal{M}_{b,J} = -16.5$ in agreement with those existing in a typical field galaxy redshift survey such as the Stromlo-APM (see Loveday *et al.* 1992). Likewise, we draw as many galaxies as we need so that those passing the surface brightness and flux criteria will approximately match the number of galaxies used by Loveday *et al.* (1992) for their luminosity function determination. In the next set of figures, we will fix $\epsilon = 0.8$ and $\beta = 400$, unless explicitly stated otherwise. The choice of these values will be justified later, in sections 3.2 and 3.3.

3. Sensitivity to the parameters

3.1. Radial expansion

Figure 1 shows quite straightforwardly the lowering of surface brightness : as mass loss due to supernova-

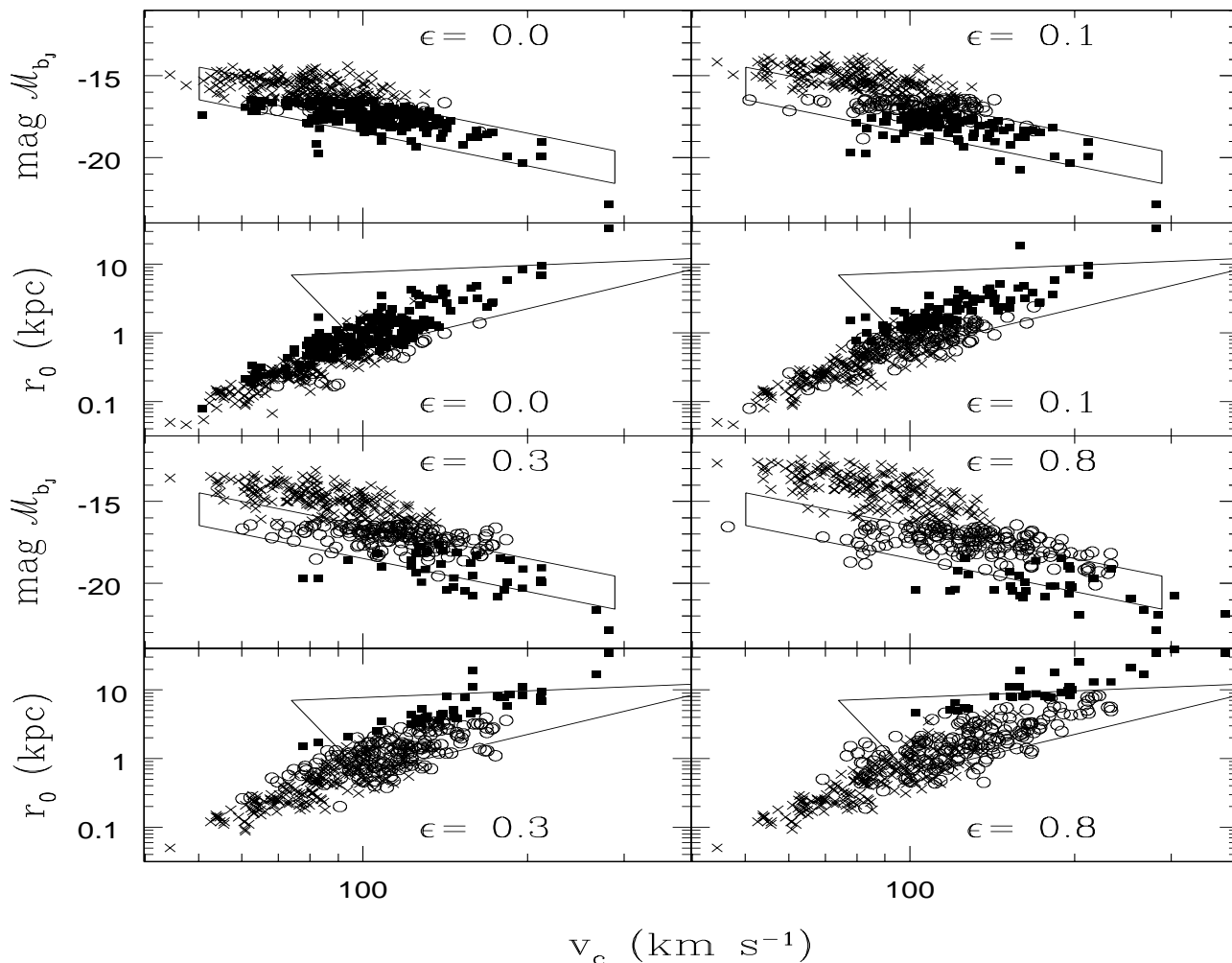


Fig. 3. Tully–Fisher relation (upper panels for each ϵ) and typical scale length as a function of circular velocity (lower panels for each ϵ) for model galaxies. Boxes indicate observational values reported by Kraan-Korteweg, Cameron & Tammann (1988; upper panels), and Courteau (1996, 1997; lower panels). The wind efficiency coefficient ϵ is taken equal to (a) 0, (b) 0.1, (c) 0.3, and (d) 0.8. Symbols are the following : crosses note objects that do not pass the flux and surface brightness threshold criteria, while objects that fulfill these constraints are represented both by circles - objects with $B - V > 0.85$ - or by squares - bluer $B - V \leq 0.85$ galaxies.

driven winds occurs, subsequent radial expansion naturally causes dimming. The objects that undergo larger radial expansion and higher mass loss are mainly the “dwarfs” (with small size and mass). However, there is also a fraction of galaxies with higher masses that become “invisible” (through a significant radial expansion). These could be the “Malin 1 type” extended disks with faint surface brightnesses that we were referring to previously.

Note that if we were to enhance the strength and frequency of winds (by adopting higher ϵ values) during a galaxy’s lifetime, the radial expansion would be more pronounced and final radii could reach up to 20 kpc. For the same reason, the μ_{be} relation (lower panel of figure 1) would also appear more scattered.

Figure 2 shows different time scales against both halo mass and blue luminosity. In general, there does seem to be a value of the halo mass that acts as a limit for “visibility” : low-mass objects (say below $10^{11.5} M_{\odot}$) are not bright enough (in magnitude nor in surface brightness) to be “observed”. However, the representation of figure 2 leaves out the most massive and high luminosity but low surface brightness objects such as those of the type of Malin 1 with $L_B \simeq 1.9 \times 10^{11} L_{B\odot}$, $\mu_e = 22.2 \pm 0.2$ V-mag/arcsec² (Bothun *et al.* 1987), but it does show (as filled circles) a less extreme class of objects : the typical giant low surface brightness spiral galaxies observed by Sprayberry *et al.* (1995) with $1.06 \times 10^{10} \leq L_B \leq 2.3 \times 10^{11} L_{B\odot}$, $21.17 \lesssim \mu_e \lesssim 26.32$ B-mag arcsec⁻². In

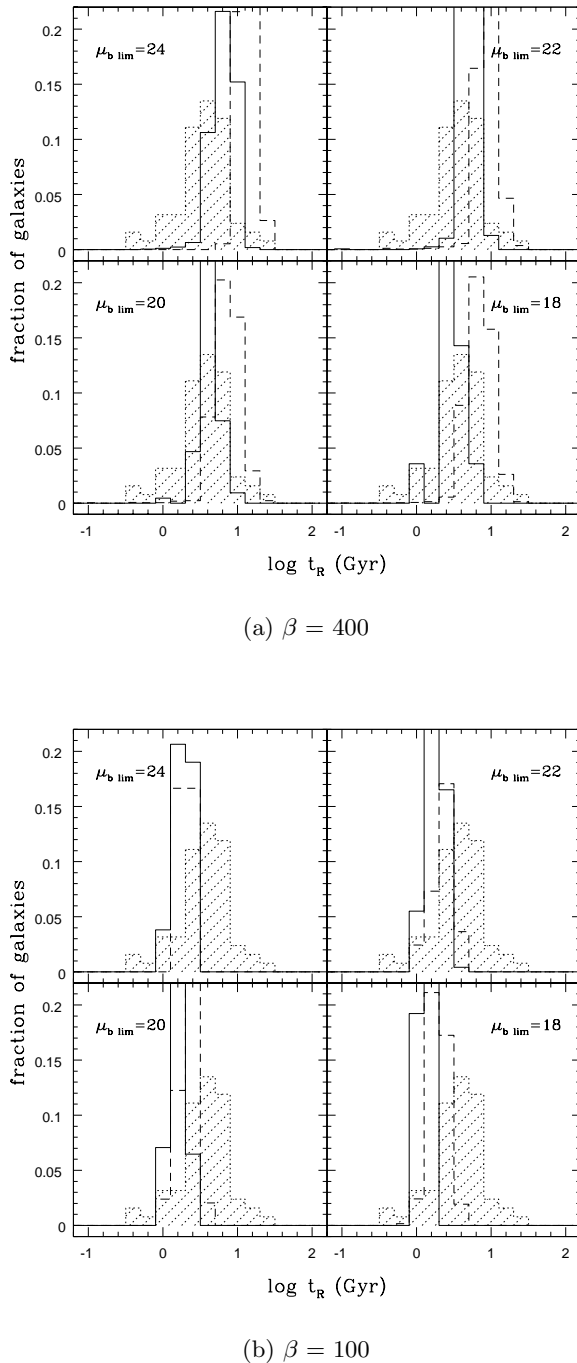


Fig. 4. Comparison between the observed distribution for the Roberts time (by Kennicutt *et al.* 1994) – hatched histogram – with distributions issued by our model for two different values of β , given below each set of figures. The histogram drawn with a continuous line is for objects that pass both magnitude and surface brightness thresholds, whereas fainter objects that fail to pass these criteria are represented by the dashed-line histogram. The surface brightness limit (in b_J magnitudes arcsec $^{-2}$ at effective radius) is indicated for each case. The ϵ parameter is fixed at 0.1.

fact, this type of galaxies can be considered to be somewhat rare (from observations) and this seems to be supported by the results of our model, which predicts that, for $L_B \gtrsim 10^{10} L_{B\odot}$, the number density of low surface-brightness objects (with $\mu_B \geq 24$ mag arcsec $^{-2}$) is only $\sim 1\%$ of the population with a high surface brightness. Finally, one should note that some galaxies suffer no wind at all during their entire lifetime (e.g. $\sim 10\%$ for “visible” ones). The objects with wind are plotted in the bottom panels of figure 2.

3.2. Feedback efficiency ϵ

Figure 3 shows both the Tully–Fisher relation (TF) and the disk size versus circular velocity relation adopted for typical late-type galaxies. We display four cases of our model results : no wind, $\epsilon = 0$; an $\epsilon = 0.1$ low-wind efficiency scenario; an intermediate case $\epsilon = 0.3$; and an $\epsilon = 0.8$ strong-wind possibility. In each figure we have limited by boxes the regions corresponding to the values observed by, respectively, Kraan-Korteweg, Cameron & Tammann (1988) for the TF relation of spirals (notice that their data are consistent with $H_0 = 57$ km $^{-1}$ Mpc $^{-1}$ and are rescaled to our $H_0 = 50$ km $^{-1}$ Mpc $^{-1}$ adopted value), and Courteau (1996, 1997) for the disk-velocity relation for a sample of nearby normal spirals. In this set of plots we separate model galaxies by colors, setting the border at $B - V = 0.85$, which is the typical color of S0 galaxies at $z = 0$ (Fukugita *et al.* 1995).

We see from figure 3 that the $\epsilon = 0$ model is the one that reproduces best the general trend and dispersion of the observations for large disks, in spite of a theoretical scatter which seems to be too large. We would thus tend to prefer this value although up to $\epsilon = 0.1$ we still get a crude agreement of the model with the observations. It is well-known that the theoretical fit to these relations is not straightforward. In particular, the steep luminosity function that theoretical models produce in the standard CDM is intimately linked to the difficulty to fit the Tully–Fisher relation with such models (Kauffmann *et al.* 1994; Cole *et al.* 1994; Somerville & Primack 1998). But, in spite of these shortcomings, we do seem to manage to obtain a generally good relation between the dynamics and the photometry, as is patent in this ensemble of figures : we have the correct galactic luminosities inside the halos, and these galaxies have the correct size (radii). This last point is crucial for surface brightness considerations once we discuss the predictions for the luminosity functions.

3.3. Star formation efficiency

The Roberts time (Kennicutt *et al.* 1994) gives an indication of the future star formation time scale of a galaxy at time t_0 :

$$t_R(t_0) = \frac{M_{gas}(t_0)}{\psi(t_0)} \quad (18)$$

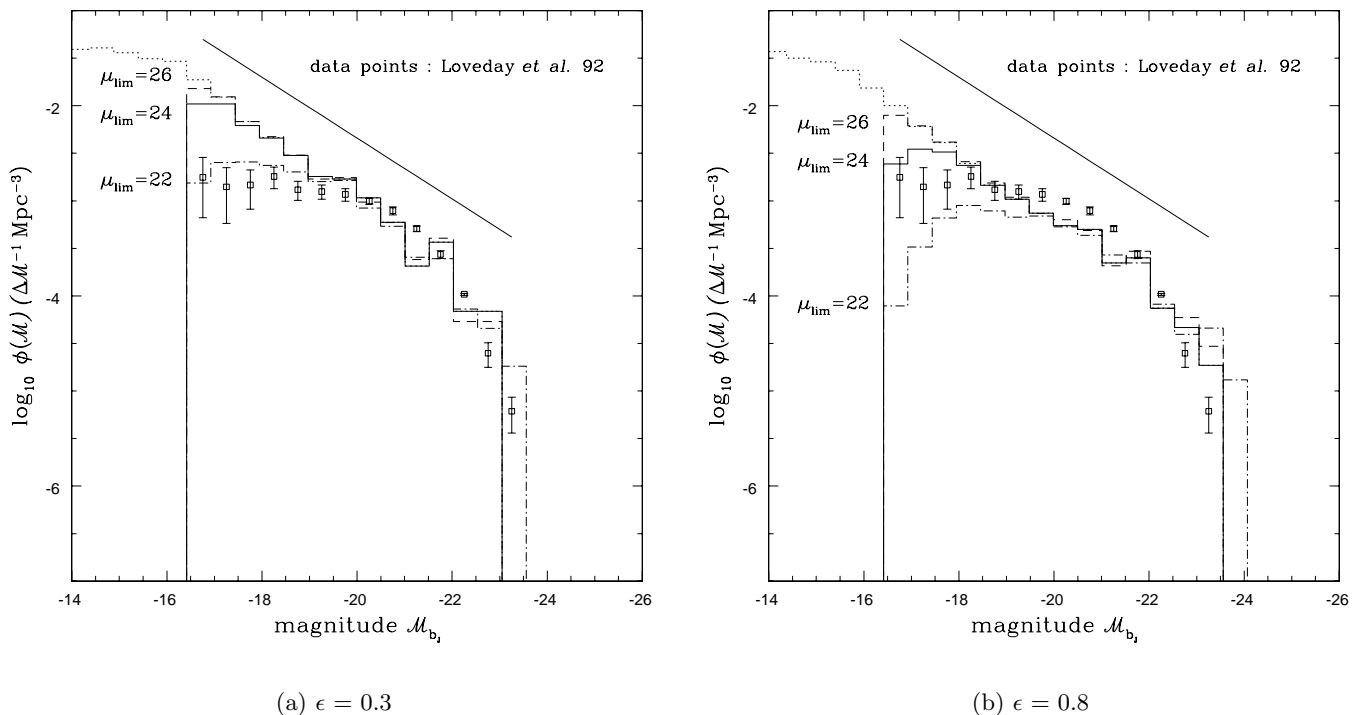


Fig. 5. Luminosity function normalized per Mpc^3 and per magnitude bin in the b_J band. Observations (by Loveday *et al.* 1992; data points) have been superimposed to the models (histograms) for (a) $\epsilon = 0.3$, (b) $\epsilon = 0.8$. The histograms with the dot-dashes, solid line and dashes indicate model galaxies that pass the survey flux limit, as well as the surface brightness limit that is indicated near each histogram for the respective mock luminosity function. The number of galaxies is approximately equal to the value reported for the observations. The histogram with the dotted line shows the model galaxy distribution as issued before submission to these selection criteria (that is for all galaxies, none excluded). The slope $\alpha = -1.8$ of the Coma cluster luminosity function as determined by Lobo *et al.* (1997) is also represented (straight line).

$\psi(t_0)$ here is either given by equation 11 (with $t = t_0$) or null if the Toomre instability criterium (Toomre 1964) is not verified, that is, if the gas surface density does not overcome Σ_c (see section 2.3).

We thus computed the Roberts time for a set of model galaxies and compared its distribution with that observed by Kennicutt *et al.* (1994) for a sample of about 60 disk galaxies. The value of the ϵ parameter was left constant at 0.1, as a result from section 3.2. This procedure provided us with the best value for the constant β , which we finally fixed at 400 – see figure 4. Because we do not know the surface brightness threshold for the Kennicutt *et al.* data, we cannot determine a unique possibility for the fit, and consequently for β . But the degeneracy thus created is not limiting, as is illustrated in each panel of figure 4a, where different realizations of the model for different surface brightness thresholds – but the same value for β – are compared to the observed data. The distribution of Roberts times does not seem to depend too much on the surface brightness threshold. The Kennicutt *et al.* limit

in surface brightness seems to lie around $20 - 22 b_J \text{ mag arcsec}^{-2}$, as estimated for $\beta = 400$.

4. Predictions for the luminosity functions in the local Universe

Galaxy luminosities computed with the model allow us to build synthetic luminosity functions at low redshift and in different photometric bands. These will be compared with observational results in this section.

4.1. Effect of ϵ

In figure 5, the normalized luminosity function per Mpc^3 and per magnitude interval, as issued by the model, is compared with observations for field and cluster galaxies.

We assume that all objects fainter than a given surface brightness detection limit will not be observed. The figure shows that, for bright galaxies, this threshold is not constraining, as one would expect, but the faint part of the luminosity function is significantly modified for different surface brightness limits. This change is translated into a

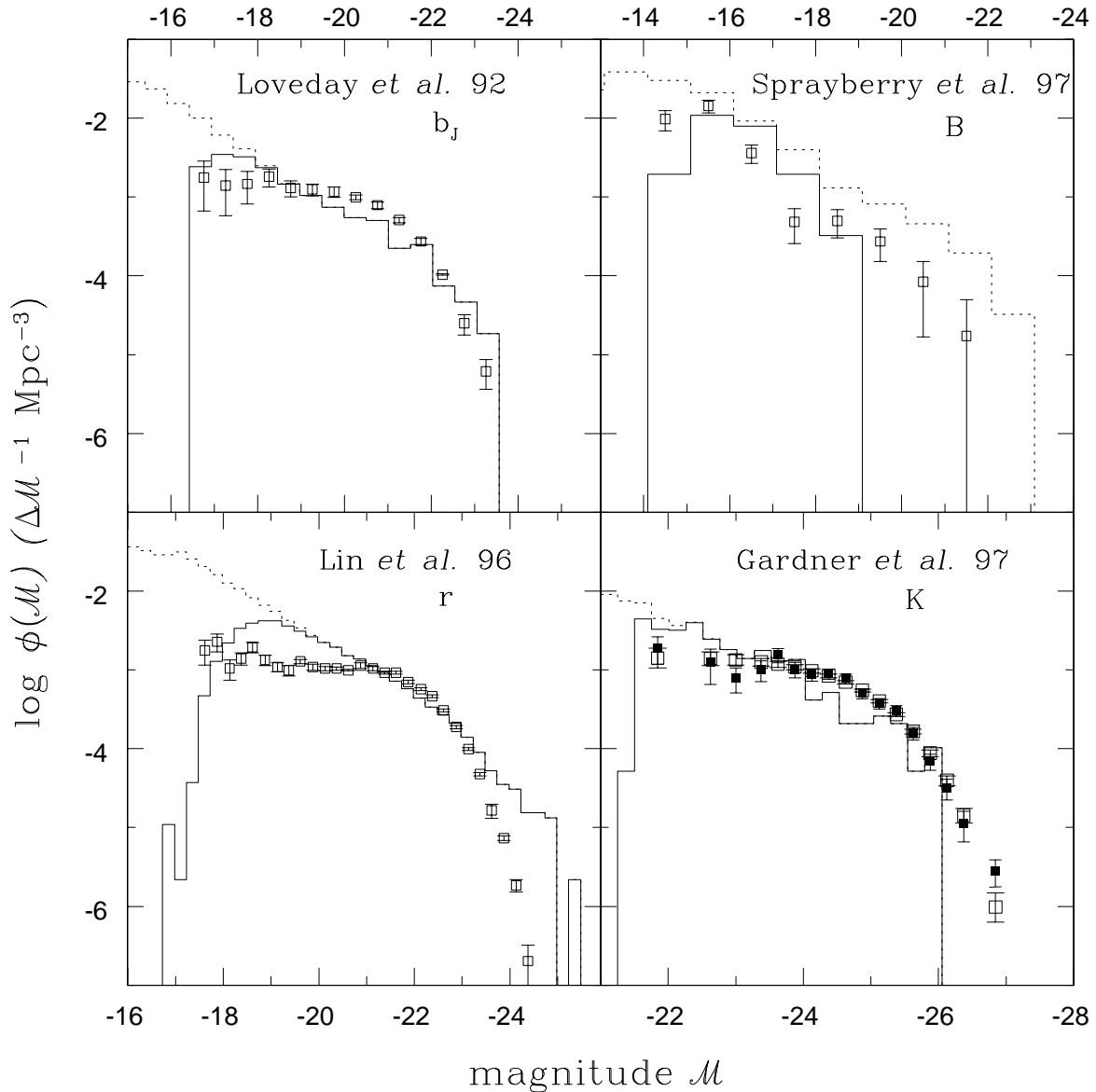


Fig. 6. Same figure as 5b ($\epsilon = 0.8$) for four different photometric wavebands. Observations (data points) available in each filter are also displayed for comparison. Surface brightness and flux limiting criteria applied to the simulations are approximately the ones reported by each survey (see text).

flattening of the histogram that gets more pronounced as the critical threshold gets more severe. Data points from Loveday *et al.* (1992) are also displayed in the same figure for comparison.

It is well-known that, with the standard CDM model, the simultaneous fit of the Tully–Fisher relation and luminosity function is difficult, because there are too many haloes (see e.g. Kauffmann *et al.* 1993). This is still true when surface-brightness effects are taken into account, with the crude modelling of supernova feedback. Even if the $\epsilon = 0.3$ model, which is already inconsistent with TF, accompanies best the part of the observational data

around \mathcal{M}^* (panel a), it fails to reproduce the faint end slope with the surface brightness limit reported by Loveday and collaborators for their survey (around $24.5 b_J$ mag arcsec $^{-2}$). Setting $\epsilon = 0.8$ allows a much better description for the “dwarf” population as figure 5b reveals. As a matter of fact, results are highly sensitive to the value of ϵ and this work might hint that ϵ changes along the luminosity sequence, but this simply illustrates that modelling galactic winds is quite a complex task, not yet fully accomplished with a single free parameter. Still, we shall consider that $\epsilon = 0.8$ gives a very reasonable and general

representation of the faint end of field galaxy luminosity functions.

Figure 5 also shows the slope $\alpha = -1.8$ of the Coma cluster luminosity function as determined by Lobo *et al.* (1997) in the V band up to magnitude $\mathcal{M}_V \simeq -14.5$ with limiting central surface brightness estimated as $\mu_V(0) = 24.5$ mag arcsec⁻². Note that, if we take $B - V = 1$ as a mean colour index for Coma galaxies (mainly ellipticals), and the simple relation connecting the surface brightness at effective radius to the central surface value, that is $\mu_e = \mu(0) + 1.127$, we get $\mu_{b_J} \sim 26.4$ mag arcsec⁻² for the practical threshold. The normalisation for the Coma data is arbitrary. It is true that we can only take this slope as indicative, as it was determined in a different waveband. Nevertheless, the similarity of it with the shape of the $\mu_{lim} = 26$ mag arcsec⁻² model histogram is quite striking, for $\epsilon = 0.3$ as well as $\epsilon = 0.8$.

4.2. Effect of μ within a given filter and looking at different wavebands

Given all these considerations, we will henceforth fix the ϵ parameter to 0.8, to reproduce the faint-end of the luminosity function. Figure 6 gives the model results convolved with four different filters. For each simulation we have applied flux and surface brightness limits corresponding to what was indicated by the authors of the respective observations. Thus, we have adopted the following thresholds: $\mathcal{M}_{b_J} = -16.5$ and $\mu_{b_J} = 24$ mag arcsec⁻² for Loveday *et al.* (1992) at $z = 0$; $-14 \leq \mathcal{M}_B \leq -22$ and $23.1 \leq \mu_B \leq 26.1$ for the deeper observations of Sprayberry *et al.* (1997), still in a blue waveband and at $z = 0$; $\mathcal{M}_K = -21.5$ and $\mu_I = 22$ mag arcsec⁻² for the K-band survey (selected in I) of Gardner *et al.* (1997) at mean redshift $z = 0.14$; and $\mathcal{M}_r = -17.5$ and $\mu_r = 22.2$ mag arcsec⁻² for the Lin *et al.* (1996) r_{Gunn} -type filter at mean redshift $z = 0.1$. Do notice that these values are indicative and a margin of ± 0.5 mag arcsec⁻² is allowed by the robustness of our models, as can be seen in figure 5. This should give us some margin to deal with uncertainties in the values estimated by the authors and with our choice of approximating the threshold to the value at effective radius. In each case, simulations were performed as many times as necessary to draw the same number of “observable” galaxies as the one reported by the respective surveys (1769 galaxies for Loveday *et al.* 1992; 693 galaxies for Sprayberry *et al.* 1997; 510 galaxies for Gardner *et al.* 1997; and 18678 for the Las Campanas survey of Lin *et al.* 1996). In doing so, we get Poisson scatters combined with intrinsic features of the luminosity functions that compare to the observational features and error bars.

The overall match at the faint end between data and simulations taking into account observational biases is quite remarkable, given the crudeness of our assumptions in this heuristic model. The rough consistency obtained for different wavebands probably unveils the presence of

the same underlying galaxy population, despite the fact that different filters preferentially sample different stellar populations.

5. Summary and Conclusions

This heuristic work shows how observational selection effects – especially surface brightness thresholds that are mainly present in field surveys – could affect the predictions of semi-analytic models of galaxy formation and evolution. In particular, we illustrate the importance of these biases in the determination of the TF relation and luminosity functions, and we confirm that they do seem to contribute to the apparent mismatch between current models of galaxy formation and a host of observations.

With our simple model, we show that, while the star formation efficiency parameter β can be fixed in a robust way, that is, independently of the adopted surface brightness limit, the same is no longer true for the wind efficiency parameter ϵ . In fact, we have shown the strong sensitivity of the results to the unknown galactic wind intensity. Once we adopt the standard one-parameter model for the feedback, we find that this parameter is likely to vary along the luminosity sequence. As a first guess, we suggest taking $\epsilon \leq 0.1$ for bright disks (according to the TF results, and loose theoretical considerations) and $\epsilon = 0.8$ to match the faint end of the luminosity functions, that is, for field “dwarfs” and for the faint galaxy population, both in the field as well as in clusters. Further research needs to be done in order to reach a more refined description of this mechanism and improve theoretical models, especially in their interplay with surface brightness effects. In particular, simulations of observations are necessary to take into account the effects of surface brightness that are more subtle than a simple “cut-off”.

The main point of the paper is the following: The standard modelling of supernova feedback via mass loss due to galactic winds is highly uncertain. Taking into account surface-brightness effects in a simple way already reveals the strong sensitivity of the results to the feedback. Still, the results are in reasonable agreement with the observations. The crude fit of the data with this type of theoretical luminosity functions – at different surface brightness thresholds and at different wavelengths – in spite of the uncertainties of the model, appears rather puzzling. It suggests that the discrepant waveband luminosity functions probably unveil the same underlying galaxy population.

Clearly more work has to be dedicated to this issue. A realistic feedback theory is still needed for a robust modelling of faint galaxies in the semi-analytic approach. In any case, the introduction of surface-brightness biases into theoretical predictions, and more specifically into the fashionable semi-analytic models of galaxy formation and evolution, is highly desirable, no less than is the careful estimate and description of the actual surface brightness threshold by observers.

Acknowledgements. We are very grateful to J. Gardner for kindly providing us with the K-band luminosity function table data from Gardner *et al.* (1997) prior to publication. CL greatly thanks E. Bertin for the very helpful discussions. Finally, we are grateful to an anonymous referee for his comments that greatly helped us improve the focus and presentation of this paper. During this work CL was supported by the fellowship reference BD/2772/93RM granted by JNICT, Portugal.

References

- Babul A., Rees M.J., 1992, MNRAS 255, 346
 Baugh C.M., Cole S., Frenk C.S., 1996a, MNRAS 283, L15
 Baugh C.M., Cole S., Frenk C.S., 1996b, MNRAS 283, 1361
 Baugh C.M., Cole S., Frenk C.S., Lacey, C.G., 1997, in "Galaxy Scaling Relations: Origins, Evolution and Applications", ESO Workshop proceedings, ed. L. da Costa and A. Renzini (Springer-Verlag), p. 52
 Bothun G.D., Impey C.D., Malin D.F., Mould J.R., 1987, AJ 94, 23
 Bothun G.D., Impey C.D., McGaugh S.S., 1997, PASP 109 745
 Bressan A., Chiosi C., Fagotto F., 1994, ApJS 94, 63
 Broadhurst T.J., Ellis R.S., Shanks T., 1988, MNRAS 235, 827
 Charbonnel C., Meynet G., Maeder A., Schaerer D., 1996, A&AS 115, 339
 Cole S., Aragón-Salamanca A., Frenk C.S., Navarro J.F., Zepf S.E., 1994., MNRAS 271, 781
 Courteau S., 1996, ApJS 103, 363
 Courteau S., 1997, AJ 114, 2402
 Cowie L.L., Songaila A., Hu E.M., 1991, Nature 354, 460
 Dekel A., Silk J., 1986, ApJ 303, 39
 De Propriis R., Pritchett C.J., Harris W.E., McClure R.D. 1995, ApJ 450, 534
 Driver S.P., Phillipps S., Davies J.I., Morgan I., Disney M.J., 1994, MNRAS, 268, 393
 Driver S.P., Phillipps S. 1996, ApJ 469, 529
 Efstathiou G., 1992, MNRAS 256, 43
 Ellis R.S., Colless M., Broadhurst T., Heyl J., Glazebrook K. 1996, MNRAS 280, 235
 Fall S.M., Efstathiou G., 1980, MNRAS 193, 189
 Fall S.M., Rees M.J., 1985, ApJ 298, 18
 Fukugita M. Shimasaku K., Ichikawa T., 1995, PASP 107, 945
 Gardner J.P., Sharples R.M., Frenk C.S., Carrasco B.E., 1997, ApJL 480, 99
 Guiderdoni B., Rocca-Volmerange B., 1987, A&A 186, 1
 Guiderdoni B., Rocca-Volmerange B., 1988, A&AS 74, 185
 Guiderdoni B., Hivon, E., Bouchet, F.R., Maffei, B., 1998, MNRAS 295, 877
 Haehnelt, M.G., Rees, M.J., 1993, MNRAS 263, 168
 Heyl J.S., Cole S., Frenk C.S., Navarro J.F., 1995, MNRAS 274, 755
 Hills J.G., 1980, ApJ 225, 986
 Impey C.D., Sprayberry D., Irwin M.J., Bothun G.D., 1996, ApJS 105, 209
 Kauffmann G., 1995, MNRAS 274, 161
 Kauffmann G., 1996, MNRAS 281, 487
 Kauffmann G., White S.D.M., Guiderdoni B., 1993, MNRAS 264, 201
 Kauffmann G., Guiderdoni B., White S.D.M., 1994, MNRAS 267, 981
 Kennicutt R.C.Jr., 1989, ApJ 344, 685
 Kennicutt R.C.Jr., Tamblyn P., Congdon C.W., 1994, ApJ 344, 685
 Kennicutt R.C.Jr., 1998, in "Starbursts: Triggers, Nature and Evolution", B. Guiderdoni & A. Kembhavi (eds.), Editions de Physique/Springer-Verlag
 Kraan-Korteweg R.C., Cameron L.M., Tammann G.A., 1988, ApJ 331, 620
 Lacey C., Silk J., 1991, ApJ 381, 14
 Lacey C., Guiderdoni B., Rocca-Volmerange B., Silk J., 1993, ApJ 402, 15
 Larson R.B., 1974, MNRAS 169, 229
 Lin H., Kirshner R.P., Sheckman S.A., Landy S.D., Oemler A., Tucker D.L., Schechter P.L., 1996, ApJ 464, 60
 Lobo C., Biviano A., Durret F., Gerbal D., Le Fèvre O., Mazure A., Slezak E., 1997, A&A 317, 385
 Loveday J., Peterson B.A., Efstathiou G., Maddox S.J., 1992, ApJ 390, 338
 Loveday J., 1997, ApJ 489, 29
 Martin, C., 1996, ApJ 465, 680
 Marzke R.O., Geller M.J., Huchra J.P., Corwin H.G.Jr., 1994a, AJ 108, 437
 Marzke R.O., Huchra J.P., Geller M.J., 1994b, ApJ 428, 43
 McGaugh S.S., 1994, Nature 367, 538
 McGaugh S.S., Bothun G.D., 1994, AJ 107, 530
 McGaugh S.S., 1995, dans IAU Symposium 171 "New Light on Galaxy Evolution", ed. ou astro-ph/9507058
 McGaugh S.S., Bothun G.D., Schombert J.M., 1995, AJ 110, 573
 McGaugh S.S., 1996, MNRAS 280, 337
 Mo H.J., Mao S., White S.D.M., 1998, MNRAS 295, 319
 Navarro J.F., White S.D.M., 1994, MNRAS 267, 401
 Navarro J.F., Frenk C.S., White S.D.M., 1997, ApJ 490, 493
 Navarro J.F., Steinmetz M., 1997, 478, 13
 Phillipps S., Driver S., 1995, MNRAS 274, 832
 Press W.H., Schechter P., 1974, ApJ 187, 425
 Rocca-Volmerange B., Guiderdoni B., 1988, A&AS 75, 93
 Scalo J.N., 1986, FCPH 11, 1
 Schade D., Ferguson H.C., 1994, MNRAS 267, 889
 Schaller G., Schaerer D., Meynet G., Maeder A., 1992, A&AS 96, 269
 Somerville R.S., Primack, J.R., 1998, MNRAS, *in press*
 Sprayberry D., Impey C.D., Bothun G.D., Irwin M.J., 1995, AJ 109, 558
 Sprayberry D., Impey C.D., Irwin M.J., Bothun G.D., 1997, ApJ 482, 104
 Thornton K., Gaudlitz M., Janka H.T., Steinmetz M., 1998, ApJ 500, 95
 Toomre A., 1964, ApJ 139, 1217
 Trentham N., 1997a, MNRAS 286, 133
 Trentham N., 1997b, MNRAS 290, 334
 Trentham N., 1998a, MNRAS 293, 71
 Trentham N., 1998b, MNRAS 294, 193
 Wilson G., Smail I., Ellis R.S., Couch W.J., 1997, MNRAS 284, 915
 White S.D.M., Frenk C.S., 1991, ApJ 379, 52
 Zucca E., Zamorani G., Vettolani G. *et al.*, 1997, A&A 326, 477